



## 저작자표시-비영리-변경금지 2.0 대한민국

이용자는 아래의 조건을 따르는 경우에 한하여 자유롭게

- 이 저작물을 복제, 배포, 전송, 전시, 공연 및 방송할 수 있습니다.

다음과 같은 조건을 따라야 합니다:



저작자표시. 귀하는 원저작자를 표시하여야 합니다.



비영리. 귀하는 이 저작물을 영리 목적으로 이용할 수 없습니다.



변경금지. 귀하는 이 저작물을 개작, 변형 또는 가공할 수 없습니다.

- 귀하는, 이 저작물의 재이용이나 배포의 경우, 이 저작물에 적용된 이용허락조건을 명확하게 나타내어야 합니다.
- 저작권자로부터 별도의 허가를 받으면 이러한 조건들은 적용되지 않습니다.

저작권법에 따른 이용자의 권리는 위의 내용에 의하여 영향을 받지 않습니다.

이것은 [이용허락규약\(Legal Code\)](#)을 이해하기 쉽게 요약한 것입니다.

[Disclaimer](#)

이학석사 학위논문

이차원 물질  $\text{Fe}_3\text{GeTe}_2$ :  
변형에 따른 결정자기이방성 변화

Two-dimensional  $\text{Fe}_3\text{GeTe}_2$ :  
strain effect on magneto-crystalline anisotropy

울산대학교 대학원

물 리 학 과

김 경 혜

Two-dimensional  $\text{Fe}_3\text{GeTe}_2$ :  
strain effect on  
magneto-crystalline anisotropy




지도교수 임성현

이 논문을 이학석사학위 논문으로 제출함

2021년 02월

울산대학교 대학원  
물 리 학 과  
김 경 혜

김경혜의 이학석사학위 논문을 인준함

심사위원 홍순철   
심사위원 김상훈 (인)   
심사위원 임성현 (인) 

울 산 대 학 교 대 학 원

2021년 02월

# ABSTRACT

## Two-dimensional $\text{Fe}_3\text{GeTe}_2$ : strain effect on magneto-crystalline anisotropy

Gyeonghye Kim

In recent years, two-dimensional (2D) materials have attracted growing attention. Atomically thin materials exhibit remarkably different properties from bulk. According to Mermin-Wagner-Hohenberg theorem, no long-range magnetic order is possible in 2D. However, magnetism in 2D has been recently observed experimentally such as  $\text{CrI}_3$ ,  $\text{Cr}_2\text{Ge}_2\text{Te}_6$  and  $\text{Fe}_3\text{GeTe}_2$ .  $\text{Fe}_3\text{GeTe}_2$  has relatively higher curie temperature  $\sim 130$  K than other 2D materials. In this dissertation, we studied monolayer and bilayer  $\text{Fe}_3\text{GeTe}_2$ , more specifically strain ( $-5\% \leq \eta \leq 5\%$ ) effect on magnetic properties.

1. **Monolayer  $\text{Fe}_3\text{GeTe}_2$ :** Strain dependence of magnetism is revealed. Among two Fe sites, Fe1 shows greater change of magnetic moments more than Fe2, from  $1.53 \mu_B$  at  $-5\%$  to  $2.37 \mu_B$  at  $+5\%$  of strain. Density of states of Fe1 are compared for each strain, different magnetic moments are associated with different peak feature. Furthermore, magneto-crystalline anisotropy (MCA) is investigated, where monolayer  $\text{Fe}_3\text{GeTe}_2$  prefers perpendicular magnetization for all strains. MCA energy changes with respect to strain, where minimum value is  $0.85$  meV at  $\eta = -5\%$ , maximum value is  $4.72$  meV without strain. Band structures at  $\eta = -5\%$  and  $0\%$  are compared to analyze MCA of two strains.
2. **Bilayer  $\text{Fe}_3\text{GeTe}_2$ :** With ferromagnetic monolayer, bilayer  $\text{Fe}_3\text{GeTe}_2$  energetically prefers antiferromagnetic state without strain. Transition to ferromagnetic state occurs at  $\eta = +4.16\%$ . Besides, at compressive strain, buckling happens in Fe2-Ge plane, which results in different magnetic moments of Fe1(in) and Fe1(out). Density of states of Fe1 are investigated to study strain dependence of magnetic moments.

# Contents

Abstract

Acknowledgment

List of Tables

List of Figures

|  |           |
|--|-----------|
| <b>CHAPTER 1 Introduction</b>                                    | <b>5</b>  |
| 1.1 Magnetic materials   | 5         |
| 1.1.1 Magnetism in two-dimension                                 | 5         |
| 1.1.2 Magnetic orderings   | 6         |
| 1.2 Method of calculations                                       | 7         |
| 1.2.1 Density functional theory                                  | 7         |
| 1.2.2 Magneto-crystalline Anisotropy                             | 9         |
| 1.3 Reference  | 10        |
| <b>CHAPTER 2 Strain effect on Fe<sub>3</sub>GeTe<sub>2</sub></b> | <b>12</b> |
| 2.1 Structure  | 12        |
| 2.2 Monolayer  | 14        |
| 2.2.1 Magnetic moments of Fe                                     | 14        |
| 2.2.2 Magneto-crystalline anisotropy                             | 19        |
| 2.3 Bilayer  | 23        |
| 2.3.1 Magnetic configurations                                    | 23        |
| 2.3.2 Magnetic moments of Fe                                     | 25        |
| 2.4 Reference  | 28        |
| <b>CHAPTER 3 Conclusion</b>                                      | <b>29</b> |

## List of Figures

**Fig. 1.1.1** Ferromagnet and antiferromagnets. (a) Ferromagnet, (b) A-type antiferromagnet, and (c) G-type antiferromagnet.

**Fig. 1.2.2** Two types of magnetic direction. (a) is out of plane direction, (b) is in-plane direction.

**Fig. 2.1** Structure of  $\text{Fe}_3\text{GeTe}_2$ . Each sphere denotes as red(Fe1), blue(Fe2), green(Ge) and yellow(Te). (a) Bilayer  $\text{Fe}_3\text{GeTe}_2$ , two monolayers connected by inversion symmetry, (b) Top view, and (c) Side view of monolayer.

**Fig. 2.2.1** Density of states of Fe1 and Fe2. The red line is Fe1, blue line is Fe2.

**Fig. 2.2.2** Density of states of Fe2 in two structure. (a) different vertical scale from Fig. 2.2.1. for Fe2 in  $\text{Fe}_3\text{GeTe}_2$  for comparison purpose, (b) Fe2 in Fe2-Ge, whose structure is shown in Fig. 2.2.3.

**Fig. 2.2.3** Fe2-Ge structure by removing Fe1 and Te from  $\text{Fe}_3\text{GeTe}_2$ . Blue and green spheres denote Fe2 and Ge, respectively.

**Fig. 2.2.4** Monolayer  $\text{Fe}_3\text{GeTe}_2$  thickness (Te to Te) respect to strain. It increases (decreases) with compressive (tensile) strain.

**Fig. 2.2.5** (a) Total magnetic moments for monolayer  $\text{Fe}_3\text{GeTe}_2$  respect to strain. (b) Magnetic moment of Fe1 and Fe2 with strain. The red and blue lines are Fe1 and Fe2, respectively.

**Fig. 2.2.6** Density of states of Fe1 at strain of (a) -5, (b) 0, and (c) 5%.

**Fig. 2.2.7**  $E_{\text{MCA}}$  of monolayer  $\text{Fe}_3\text{GeTe}_2$  with strain.  $E_{\text{MCA}} > 0$  for all strains.

**Fig. 2.2.8**  $k$  resolved  $E_{\text{MCA}}$  for two representative strains (a) 0 % and (b) -5 %. Note different vertical scales of (a) and (b). Highlighted parts are for comparison of two strains. In -5 % relative to

0 %,  $E_{MCA}$  in  $\Gamma - K$  increases, while that in  $M - \Gamma$  decreases.

**Fig. 2.2.9** Band structures with orbital composition. Black stands for  $|m| = 0$ , red for  $|m| = 1$ , blue for  $|m| = 2$ , respectively. Contribution from (a) Fe1 and (b) Fe2 are distinguished. Highlight parts are same part as that of Fig. 2.2.8. Bands with occupation change under strain are denoted in yellow for Fe1 and Fe2, respectively.

**Fig. 2.3.1** Two type of  $\text{Fe}_3\text{GeTe}_2$  spin configuration. (a) A-type antiferromagnetic state, (b) ferromagnetic state. Each monolayer has ferromagnetic state.

**Fig. 2.3.2** Energy difference between FM and A-AFM,  $\Delta E = E_{FM} - E_{AFM}$ , of bilayer  $\text{Fe}_3\text{GeTe}_2$ , with respect to strain.

**Fig. 2.3.3** Structure of bilayer  $\text{Fe}_3\text{GeTe}_2$  (a) without strain and (b) with strain of -5%. In (b), with compressive strain, buckling happens in Fe2-Ge plane, where Fe2 and Ge move closer to Fe1(out) and Fe1(in), respectively. (c) Strain dependence of thickness of monolayer unit defined as distance between Fe2 z-axis position and Ge z-axis position.

**Fig. 2.3.4** Bilayer  $\text{Fe}_3\text{GeTe}_2$  magnetic moment regarding strain. Purple, red and blue lines denote Fe1(out), Fe1(in), and Fe2, respectively. Fe2 magnetic moment is little changed. Fe1(in) magnetic moment is changed more than Fe1(out), especially in compressive strain range.

**Fig. 2.3.5** Density of states of Fe1(out) and Fe1(in) at strain of (a) -5, (b) 0, and (c) 5 %. The purple and red lines are Fe1(out) and Fe1(in), respectively. (b) and (c) show similar shape of DOS between Fe1(in) and Fe1(out) but (a) does not.



# Chapter 1: Introduction

## 1.1 Magnetic materials

### 1.1.1 Magnetism in two-dimension

Magnetic material shows an ordered magnetic configuration over macroscopic length scale. This arrangement is usually driven by the exchange interaction between neighboring atoms. If temperature increases above Curie temperature ( $T_c$ ), the long-range order disappears due to thermal fluctuations. Dimensionality plays an important role in determining magnetism, which have been studied for decades. In three-dimension, magnetism can always occur at finite temperature while in one-dimension, magnetism is possible only at zero temperature [1]. On the other hand, in two-dimension is different. According to Mermin-Wagner-Hohenberg theorem [2, 3], no long-range magnetic order is possible in two-dimension. However, magnetism in two-dimension has been recently observed experimentally, for example,  $\text{CrI}_3$  [4],  $\text{Cr}_2\text{Ge}_2\text{Te}_6$  [5], and  $\text{Fe}_3\text{GeTe}_2$ . As such, in recent years, two-dimensional (2D) magnetic materials [6, 7] have received attentions for many intriguing physics and material properties.

## 1.1.2 Magnetic orderings

As mentioned above, magnetic materials show an ordered magnetic configuration. Among magnetic orderings, ferromagnet (FM) and antiferromagnet (AFM) are discussed in this section. Magnetic moments of atoms align in parallel in FM and anti-parallel in AFM state, respectively, which is shown in Fig. 1.1.1. AFM has two types, A-type and G-type. In this dissertation, FM and A-type AFM are considered for bilayer  $\text{Fe}_3\text{GeTe}_2$ .

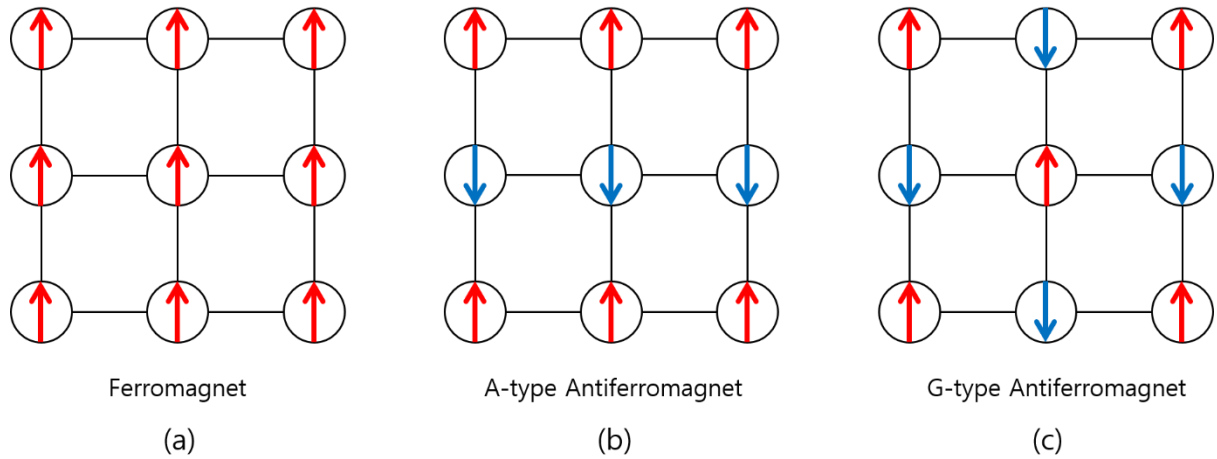


**Fig. 1.1.1** Ferromagnet and antiferromagnets. (a) Ferromagnet, (b) A-type antiferromagnet, and (c) G-type antiferromagnet.

## 1.2 Method of calculations

### 1.2.1 Density functional theory

Density functional theory [8-10] is used to investigate electronic structure of solids. It is initiated from Hohenberg-Kohn theorem and Kohn-Sham equations. In many-electron system, the energy can be written as

$$E = \langle \Psi | \hat{H} | \Psi \rangle = \int d\vec{r}_1 \dots d\vec{r}_N \Psi^*(\vec{r}_1, \dots, \vec{r}_N) \hat{H} \Psi(\vec{r}_1, \dots, \vec{r}_N), \quad (1.2.1)$$

where

$$\hat{H}(\vec{r}_1, \dots, \vec{r}_N) = - \sum_i \frac{1}{2} \nabla_i^2 + \sum_i V_{ext}(\vec{r}_i) + \frac{1}{2} \sum_{i \neq j} \frac{1}{|\vec{r}_i - \vec{r}_j|}, \quad (1.2.2)$$

with fixed nuclei. The first term of Eq. (1.2.2) is the kinetic energy, the second term is the external potential, and the last term is the electron-electron Coulomb energy. According to Hohenberg-Kohn theorem, the external potential of the nuclei ( $V_{ext}$ ) in the ground state is uniquely determined by electron density. Therefore, to obtain total energy,  $E$ , of the ground state, only electron density ( $n$ ) is necessary. In other words, the total energy of ground state is a functional of the electron density,

$$E[n] = \int d\vec{r} n(\vec{r}) V_{ext}(\vec{r}) + \left\langle \Psi[n] \left| - \sum_i \frac{1}{2} \nabla_i^2 + \frac{1}{2} \sum_{i \neq j} \frac{1}{|\vec{r}_i - \vec{r}_j|} \right| \Psi[n] \right\rangle. \quad (1.2.3)$$

The ground state density ( $n_0$ ) minimizes the total energy ( $E[n]$ ), in the framework of variational principle,

$$\left. \frac{\delta E[n]}{\delta n} \right|_{n_0} = 0. \quad (1.2.5)$$

Now we discuss how to construct such functional ( $E[n]$ ), Kohn and Sham equation. In Eq. (1.2.3), Kohn and Sham introduced non-interacting particles  $\phi_i(\vec{r})$ , which split the kinetic, coulomb energy term and an extra term:

$$E[n] = \int d\vec{r} n(\vec{r}) V_{ext}(\vec{r}) - \sum_i \int d\vec{r} \phi_i^*(\vec{r}) \frac{1}{2} \nabla_i^2 \phi_i(\vec{r}) + \frac{1}{2} \int \int d\vec{r} d\vec{r}' \frac{n(\vec{r})n(\vec{r}')}{|\vec{r} - \vec{r}'|} + E_{xc}[n]. \quad (1.2.6)$$

In Eq. (1.2.6), the first three terms are the external potential, the kinetic energy, and the Hartree energy, respectively, where the last term,  $E_{xc}[n]$ , is the exchange-correlation energy,

$$E_{xc}[n] = E_x[n] + E_c[n] = \int d^3r n(\vec{r}) \varepsilon_x[n(\vec{r})] + \int d^3r n(\vec{r}) \varepsilon_c[n(\vec{r})]. \quad (1.2.7)$$

If  $E_{xc}[n]$  is known, the total energy of the system in ground state can be determined from the electron density. As  $E_{xc}$  is not exactly known, two approximations are used for  $E_{xc}[n]$ : one is the local density approximation (LDA) and the other one is the generalized-gradient approximations (GGA). The idea of LDA is that the homogeneous electron gas,  $n^\uparrow(\vec{r}) = n^\downarrow(\vec{r}) = n(\vec{r})/2$ , is used to describe the exchange and correlation energy of real system with regions with slowly varying density. For magnetic system, local spin density approximation (LSDA) is used. LSDA considers spin polarization ( $\xi$ ), and  $E_{xc}[n]$  can be written as,

$$\xi(\vec{r}) = \frac{n^\uparrow(\vec{r}) - n^\downarrow(\vec{r})}{n(\vec{r})}, \quad (1.2.8)$$

$$E_{xc}^{LSDA}[n^\uparrow, n^\downarrow] = \int d^3r n(\vec{r}) [\varepsilon_x(n^\uparrow(\vec{r}), n^\downarrow(\vec{r})) + \varepsilon_c(n^\uparrow(\vec{r}), n^\downarrow(\vec{r}))]. \quad (1.2.9)$$

However, LDA has shortcomings such as underestimate of chemical bond energies, bond lengths, and lattice constants. To overcome this limitation, not only the electronic density but also gradient of the density ( $|\nabla n|$ ) is considered. To deal with this, the generalized-gradient approximations (GGA) is proposed,

$$E_{xc}^{GGA}[n^\uparrow, n^\downarrow] = \int d^3r n(\vec{r}) \varepsilon_{xc}(n^\uparrow(\vec{r}), n^\downarrow(\vec{r}), |\nabla n^\uparrow|, |\nabla n^\downarrow|, \dots). \quad (1.2.10)$$

GGA generally gives better result than LDA (LSDA) in calculating some properties of materials (lattice constant, bond length, and binding energies ...). With these two approximations (LSDA, GGA), density functional theory has been successful in theoretical research.

## 1.2.2 Magneto-crystalline Anisotropy

Magneto-crystalline anisotropy (MCA) is a tendency of magnetization to align along a favored direction [11]. MCA energy ( $E_{\text{MCA}}$ ) is the difference of energy between when magnetization directing in-plane and out of plane (Fig. 1.2.2), where positive (negative) value indicates perpendicular (in-plane) magnetization,

$$E_{\text{MCA}} = E_{\parallel} - E_{\perp}. \quad (1.2.11)$$

Force theorem has been used in calculation of MCA energy [12], sum of energy eigenvalues of two different magnetization. Here,  $k$  resolved formula is used,

$$E_{\text{MCA}}(\mathbf{k}) = \sum_{n \in \text{occ}} [E(n, \mathbf{k})^{\parallel} - E(n, \mathbf{k})^{\perp}]. \quad (1.2.12)$$

Furthermore, in the framework of the perturbation theory [13],  $E_{\text{MCA}}$  is expressed as spin-orbit coupling (SOC) between occupied and unoccupied states,

$$E_{\text{MCA}} = \xi^2 \sum_{o,u} \frac{|\langle m_o, \sigma_o | L_z | m_u, \sigma_u \rangle|^2 - |\langle m_o, \sigma_o | L_x | m_u, \sigma_u \rangle|^2}{E_{u, \sigma_u} - E_{o, \sigma_o}}. \quad (1.2.13)$$

$\xi$  is the amplitude SOC;  $\sigma_o(\sigma_u)$  is spin of occupied(unoccupied) state;  $m$  is magnetic quantum number;  $L_z$  ( $L_x$ ) is the angular momentum operator for perpendicular (in plane) direction, respectively;  $E_{u, \sigma_u}$  and  $E_{o, \sigma_o}$  are energies of unoccupied and occupied states.



**Fig. 1.2.2** Two types of magnetic direction. (a) is out of plane direction, (b) is in-plane direction.

## 1.3 Reference

- [1] R. Peierls, Math. Proc. Cambridge Philos. Soc **32**, 477 (1936).
- [2] N. D. Mermin and H. Wagner, Phys. Rev. Lett. **17**, 1133 (1966).
- [3] P. C. Hohenberg, Phys. Rev. **158**, 383 (1967).
- [4] Bevin Huang, Genevieve Clark, Efrén Navarro-Moratalla, Dahlia R. Klein, Ran Cheng, Kyle L. Seyler, Ding Zhong, Emma Schmidgall, Michael A. McGuire, David H. Cobden, Wang Yao, Di Xiao, Pablo Jarillo-Herrero and Xiaodong Xu, Nature **546**, 270 (2017).
- [5] Cheng Gong, Lin Li, Zhenglu Li, Huiwen Ji, Alex Stern, Yang Xia, Ting Cao, Wei Bao, Chenzhe Wang, Yuan Wang, Z. Q. Qiu, R. J. Cava, Steven G. Louie, Jing Xia and Xiang Zhang, Nature **546**, 265 (2017).
- [6] Kenneth S. Burch, David Mandrus and Je-Geun Park, Nature **563**, 47 (2018).
- [7] M. Giberini, M. Koperski, A. F. Morpurgo and K. S. Novoselov, Nat. Nanotechnol. **14**, 408 (2019).
- [8] Feliciano Giustino, *Materials Modelling using Density Functional Theory: Properties and Predictions*, Oxford University Press (2014).
- [9] Richard M. Martin, *Electronic Structure: Basic Theory and Practical Methods*, Cambridge University Press (2004).
- [10] Robert G. Parr and Weitao Yang, *Density-Functional Theory of Atoms and Molecules*, Oxford University Press (1989).
- [11] Nicola A. Spaldin, *Magnetic Materials: Fundamentals and Applications*, Cambridge

University Press (2010).

[12] M. Weinert, R. E. Watson, and J. W. Davenport, Phys. Rev. B **32**, 2115 (1985).

[13] Ding-Sheng Wang, Ruqian Wu, and A. J. Freeman, Phys. Rev. B **47**, 14932 (1993).

## Chapter 2: Strain effect on $\text{Fe}_3\text{GeTe}_2$

In this chapter, strain effect on magnetism of monolayer and bilayer  $\text{Fe}_3\text{GeTe}_2$  (FGT) are discussed. For monolayer FGT, we discuss magnetic moments and magneto-crystalline anisotropy. For bilayer FGT, magnetic configurations are studied.

### 2.1 Structure

$\text{Fe}_3\text{GeTe}_2$  (FGT) is one of two-dimensional magnetic materials with relatively high Curie temperature (monolayer  $\sim 130$  K) [1]. It has hexagonal structure with space group  $P6_3/mmc$  (# 194), whose lattice constant is  $a = 4.00 \text{ \AA}$  and  $c = 16.39 \text{ \AA}$ . As seen in Fig. 2.1(a), bilayer consists of two monolayer units, connected by inversion symmetry as well as screw rotation. Fe is distinguished as two types, Fe1 and Fe2. Fe2 is on the same plane with Ge, while Fe1 is above and below this plane. Also,  $\text{Fe}_3\text{Ge}$  layers are sandwiched by Te. Fe1 is on A-site, Ge is on B-site, and Te, Fe2 are on C-site of hexagonal structure as shown in Fig. 2.1(b).



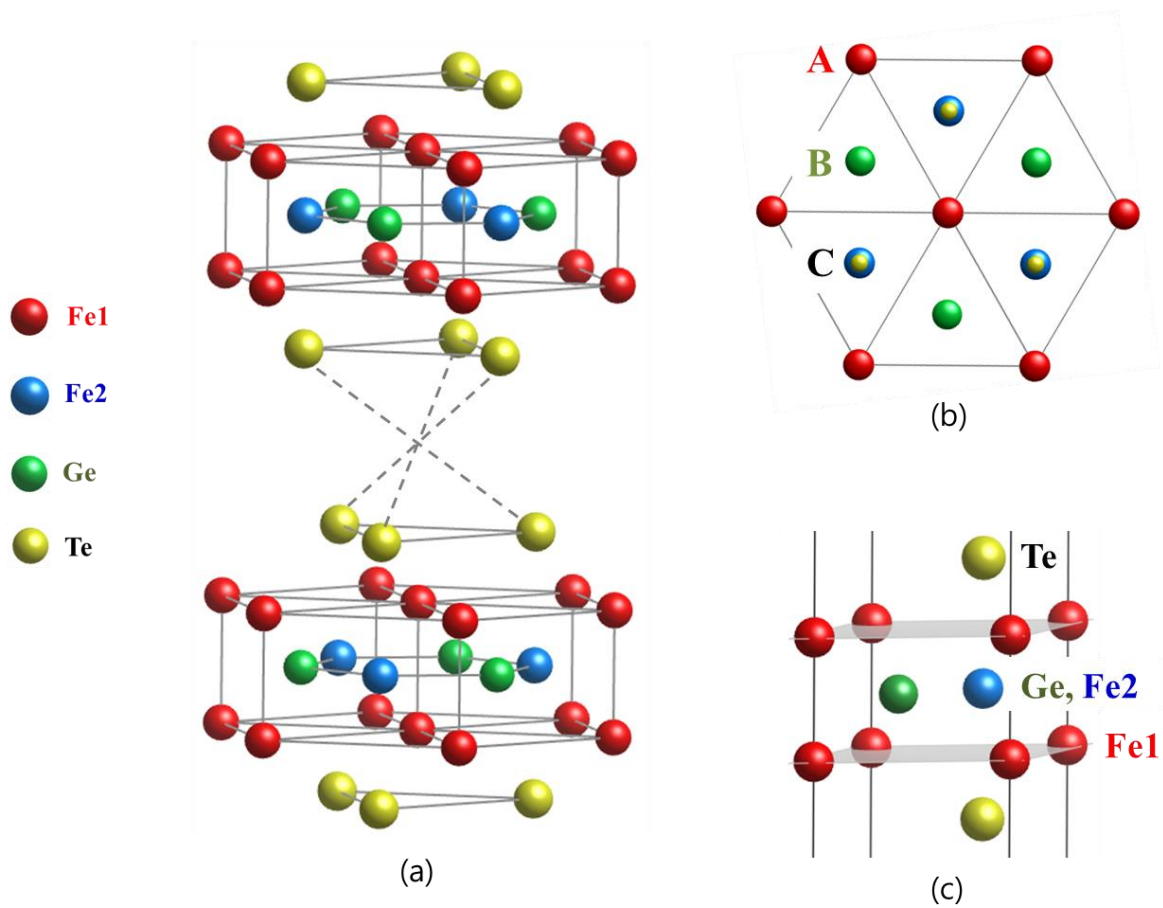


**Fig. 2.1** Structure of  $\text{Fe}_3\text{GeTe}_2$ . Each sphere denotes as red(Fe1), blue(Fe2), green(Ge) and yellow(Te). (a) Bilayer  $\text{Fe}_3\text{GeTe}_2$ , two monolayers connected by inversion symmetry, (b) Top view, and (c) Side view of monolayer.

## 2.2 Monolayer

In this section, monolayer  $\text{Fe}_3\text{GeTe}_2$  is discussed for strain dependent magnetic moments and magneto-crystalline anisotropy.

### 2.2.1 Magnetic moments of Fe

Without strain ( $\eta = 0$ ), monolayer has total magnetic moment of  $5.04 \mu_B$ , where Fe1 and Fe2 have  $2.06 \mu_B$  and  $1.04 \mu_B$ , respectively. As mentioned before, Fe2 is on the same plane with Ge, and Fe1 is above and below this plane. As such, as shown in Fig. 2.2.1, Fe1 and Fe2 show different characteristics: DOS of Fe2 has more spread feature than Fe1, which gives different magnetic moments. To see more on this difference, two DOS of Fe2 are investigated as shown in Fig. 2.2.2. One is Fe2 in the FGT structure, the same as Fig. 2.2.1, the other is when Fe2 in Fe2-Ge structure: without Fe1 and Te. Comparing the two, Fe2 has well spread DOS in the FGT but has larger peak in Fe2-Ge. Also, Fe2 in Fe2-Ge has magnetic moments around  $2.15 \mu_B$  similar to Fe1 in FGT. Therefore, it seems Fe2 reduces magnetism because of other planes.

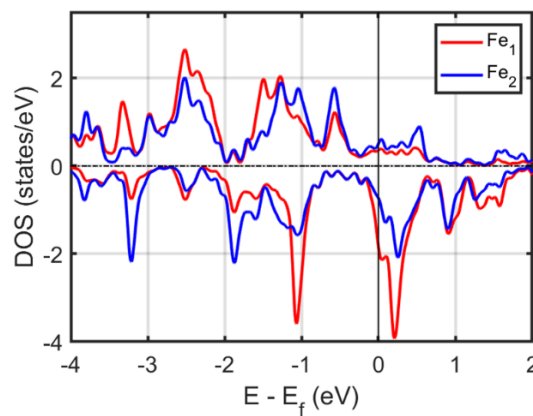


**Fig. 2.2.1** Density of states of Fe1 and Fe2. The red line is Fe1, blue line is Fe2.

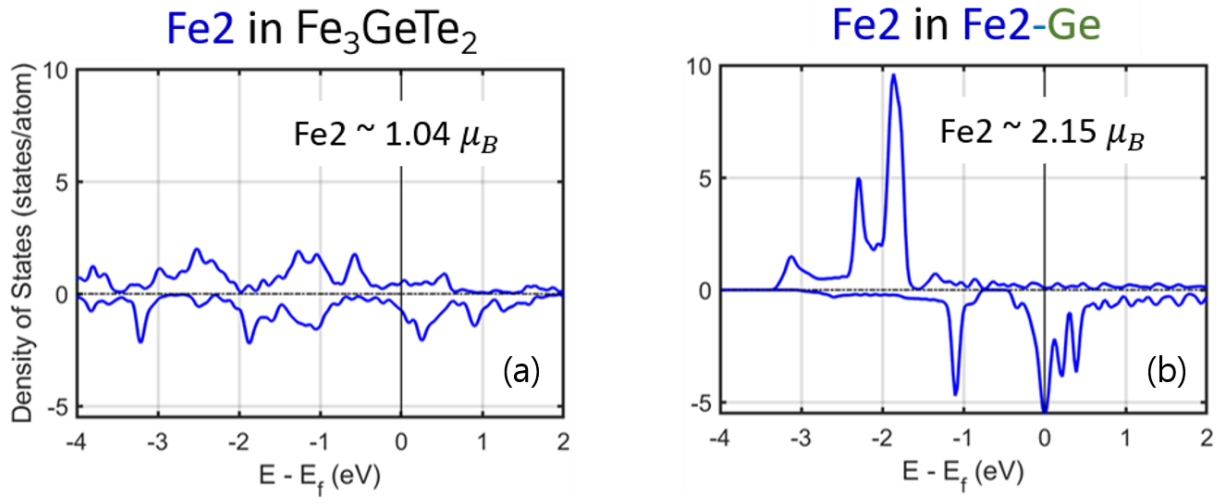


**Fig. 2.2.2** Density of states of Fe2 in two structure. (a) different vertical scale from Fig. 2.2.1. for Fe2 in  $\text{Fe}_3\text{GeTe}_2$  for comparison purpose, (b) Fe2 in Fe2-Ge, whose structure is shown in Fig. 2.2.3.

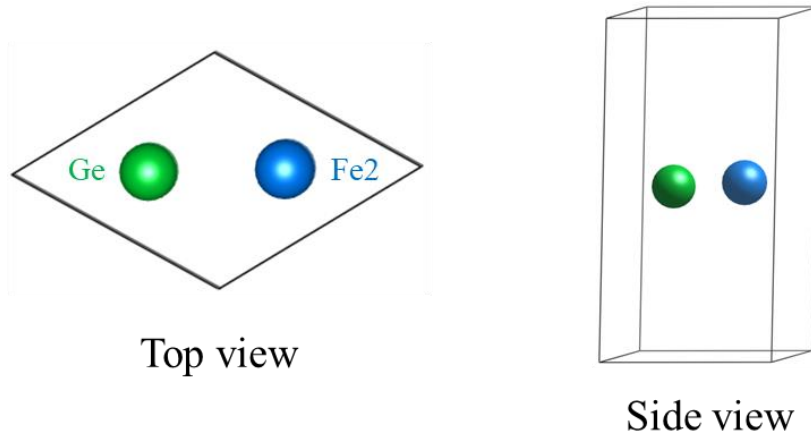


**Fig. 2.2.3** Fe2-Ge structure by removing Fe1 and Te from  $\text{Fe}_3\text{GeTe}_2$ . Blue and green spheres denote Fe2 and Ge, respectively.

As shown in Fig. 2.2.4, thickness of monolayer increases and decreases with compressive and tensile strain, respectively. Magnetic moments also change. Fig. 2.2.5 (a) shows change of total magnetic moments with strain ( $-5 \% \leq \eta \leq 5 \%$ ) where the maximum (minimum) occurs at  $\eta = 5 \%$  ( $-5 \%$ ) with  $5.72$  ( $4.07$ )  $\mu_B$ . Especially as seen in Fig. 2.2.5 (b), Fe1 magnetic moment has noticeable change from  $1.53 \mu_B$  to  $2.37 \mu_B$  for  $\eta = -5 \%$  and  $5 \%$  respectively. In this regard, DOS of Fe1 is investigated by comparing DOS at  $\eta = 0 \%$  with at  $\eta = -5$  and  $5 \%$ . As seen in Fig. 2.2.6, they have different peak feature. Peak moves to the left (occupied) at  $-5\%$  and to the right (unoccupied) at  $5\%$ , compared to strain of  $0\%$ . It is related to magnetic moments of Fe1, smaller at  $-5\%$  ( $1.53 \mu_B$ ), larger at  $5\%$  ( $2.37 \mu_B$ ) than  $0\%$  ( $2.06 \mu_B$ ).

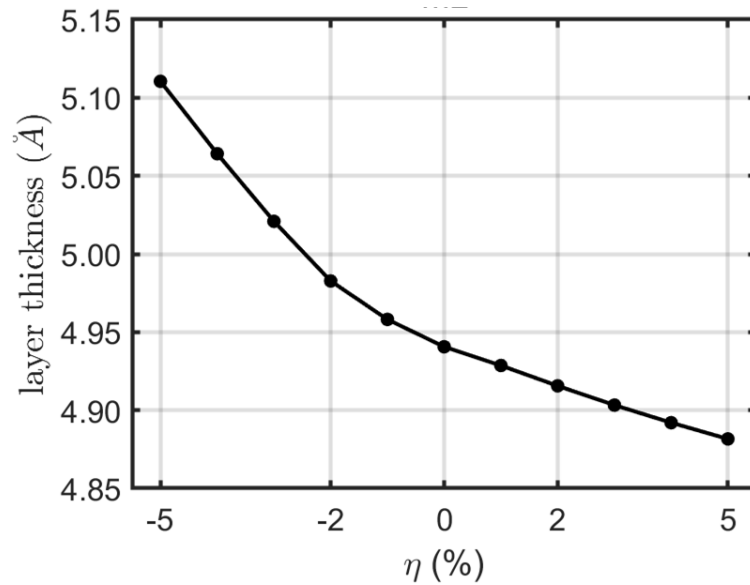


**Fig. 2.2.4** Monolayer  $\text{Fe}_3\text{GeTe}_2$  thickness (Te to Te) respect to strain. It increases (decreases) with compressive (tensile) strain.

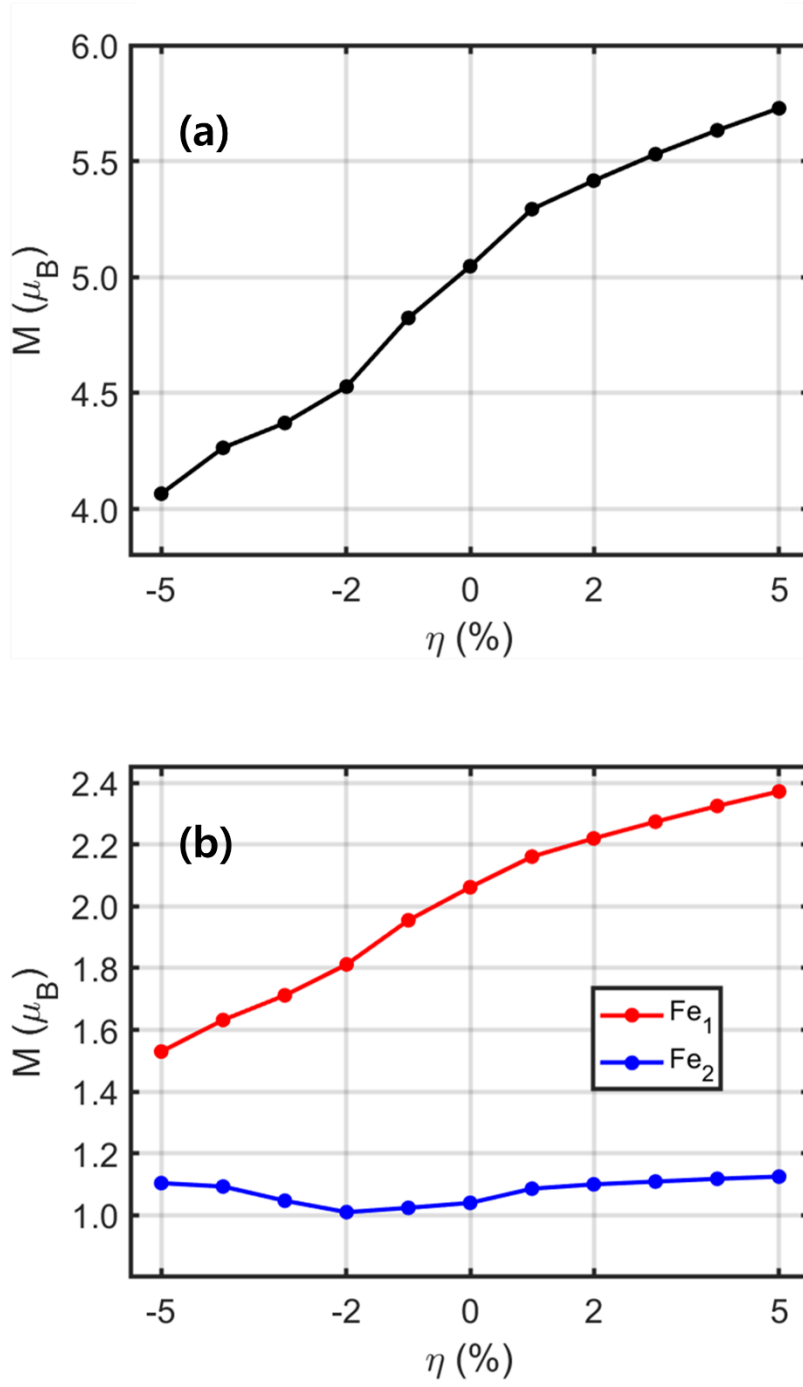


**Fig. 2.2.5** (a) Total magnetic moments for monolayer Fe<sub>3</sub>GeTe<sub>2</sub> respect to strain. (b) Magnetic moment of Fe<sub>1</sub> and Fe<sub>2</sub> with strain. The red and blue lines are Fe<sub>1</sub> and Fe<sub>2</sub>, respectively.



### 2.2.2 Magneto-crystalline anisotropy

Magneto-crystalline anisotropy (MCA) of monolayer FGT is tackled for strain of  $-5\% \leq \eta \leq 5\%$ . Energy cutoff 450 eV and  $21 \times 21 \times 1$  Monkhorst-Pack  $k$  mesh are used. LDA is used for the exchange-correlation potential. As shown in Fig. 2.2.7, monolayer FGT has perpendicular MCA (PMCA),  $E_{\text{MCA}} > 0$ , for all strains. However, magnitude of MCA changes with strain. More specifically,  $E_{\text{MCA}}$  decreases from 4.72 meV at  $\eta = 0\%$  to 0.85 and 3.49 meV for compressive and tensile strain, respectively. Compared to tensile strain, compressive strain greatly changes  $E_{\text{MCA}}$ .

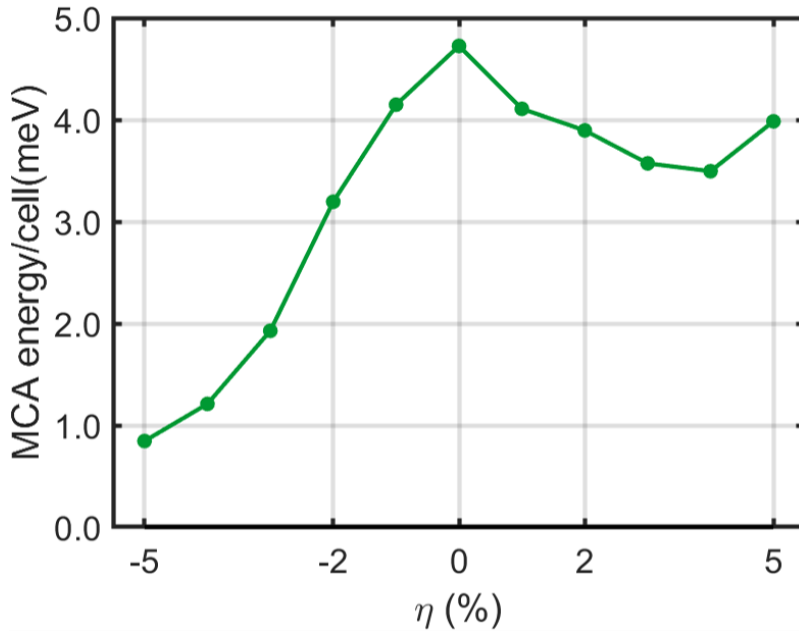


**Fig. 2.2.7**  $E_{\text{MCA}}$  of monolayer  $\text{Fe}_3\text{GeTe}_2$  with strain.  $E_{\text{MCA}} > 0$  for all strains.

To see more, we focus on two cases, at strain of 0 % and  $-5\%$ . To do so,  $k$  resolved MCA is shown in Fig. 2.2.8. As seen, the overall value decreases from 0 % to  $-5\%$ . Two parts are highlighted in Fig. 2.2.8, where MCA contribution increases and decreases at  $\Gamma - K$  and  $M - \Gamma$ , respectively, from 0 to  $-5\%$  strain.

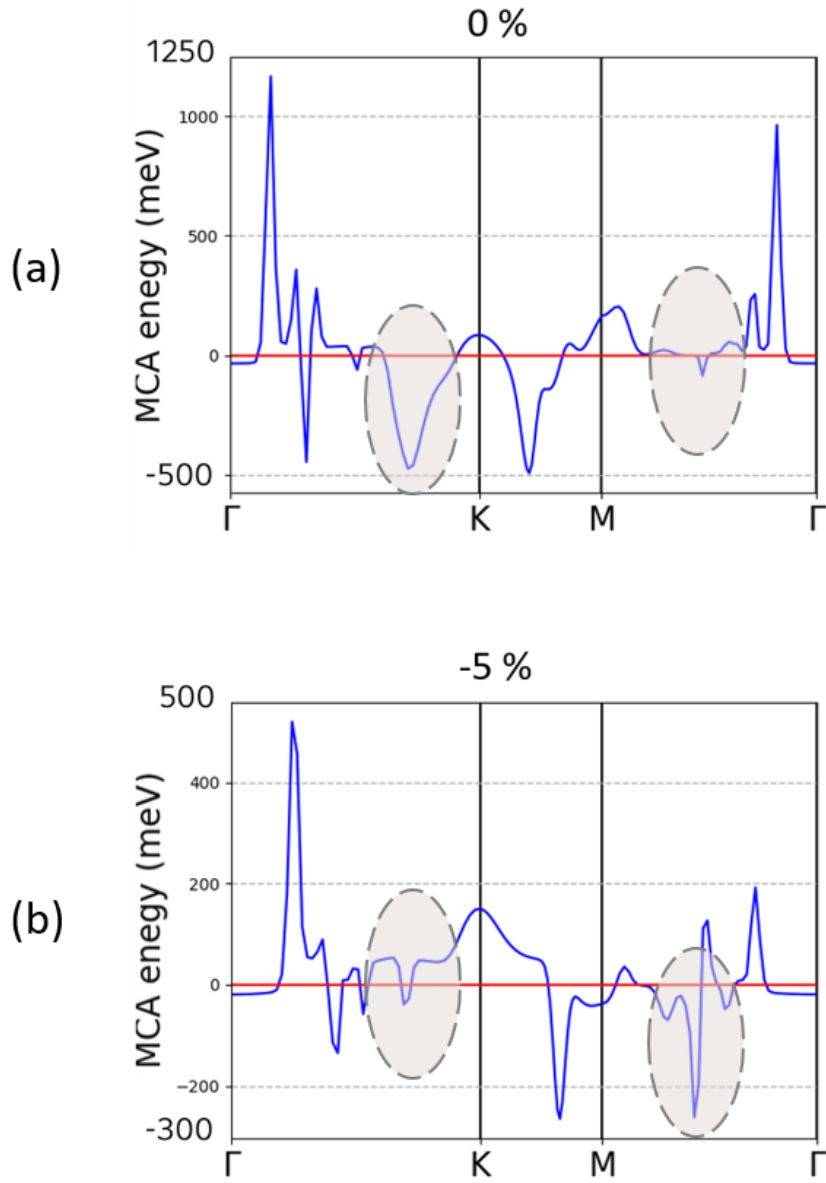


**Fig. 2.2.8**  $k$  resolved  $E_{\text{MCA}}$  for two representative strains (a) 0 % and (b) -5 %. Note different vertical scales of (a) and (b). Highlighted parts are for comparison of two strains. In -5 % relative to 0 %,  $E_{\text{MCA}}$  in  $\Gamma - K$  increases, while that in  $M - \Gamma$  decreases.



Further, band structure is plotted in Fig. 2.2.9 with  $d$ -orbital projection. In hexagonal lattice,  $d$ -orbitals are decomposed into three states,  $|m| = 0$ ,  $|m| = 1$ , and  $|m| = 2$ . In addition, contribution from Fe1 and Fe2 are distinguished at upper and lower panels, respectively. According to the perturbation theory,

$$E_{\text{MCA}} = \xi^2 \sum_{o,u} \frac{|\langle m_o, \sigma_o | L_z | m_u, \sigma_u \rangle|^2 - |\langle m_o, \sigma_o | L_x | m_u, \sigma_u \rangle|^2}{E_{u, \sigma_u} - E_{o, \sigma_o}}, \quad (2.2.1)$$

which is used to analyze MCA from band structure. As seen in Fig. 2.2.9, band changes with strain, which alters the denominator of Eq. 2.2.1. Majority spin states do not change much in this energy range of  $-0.3 \sim 0.3$  eV, which do not affect  $E_{\text{MCA}}$ .

As seen in Fig. 2.2.9 (a), band A ( $|m| = 1$ ) is unoccupied. This band does not couple with occupied state bands along  $M - \Gamma$ , highlighted with ellipse. At  $\eta = -5\%$ , band A moves to A' with occupation change. Band A' couples with band ( $|m| = 2$ ) of unoccupied state where the matrix  $\langle |m|=1 \downarrow | L_x | |m|=2 \downarrow \rangle$  contributes with  $\Delta E = 0.21$  eV for the denominator of Eq. 2.2.1.

In Fig. 2.2.9 (b), from  $\eta = 0$  to  $-5\%$ , unoccupied band B ( $|m| = 1$ ) becomes occupied as labeled B'. Along  $\Gamma - K$ , highlighted with ellipse, band B couples with occupied state band ( $|m|=2$ ) where the matrix  $\langle |m|=2 \downarrow | L_x | |m|=1 \downarrow \rangle$  contributes with  $\Delta E = 0.16$  eV for the denominator of Eq. 2.2.1.

Band B' couples with band ( $|m| = 1$ ) of unoccupied state, where the matrix  $\langle |m|=1 \downarrow | L_z | |m|=1 \downarrow \rangle$  contributes with  $\Delta E = 0.34$  eV.

One thing we want to mention here is that  $K'$  point is not studied in this dissertation. Monolayer  $\text{Fe}_3\text{GeTe}_2$  has broken inversion symmetry,  $K'$  points need to be investigated for completeness.

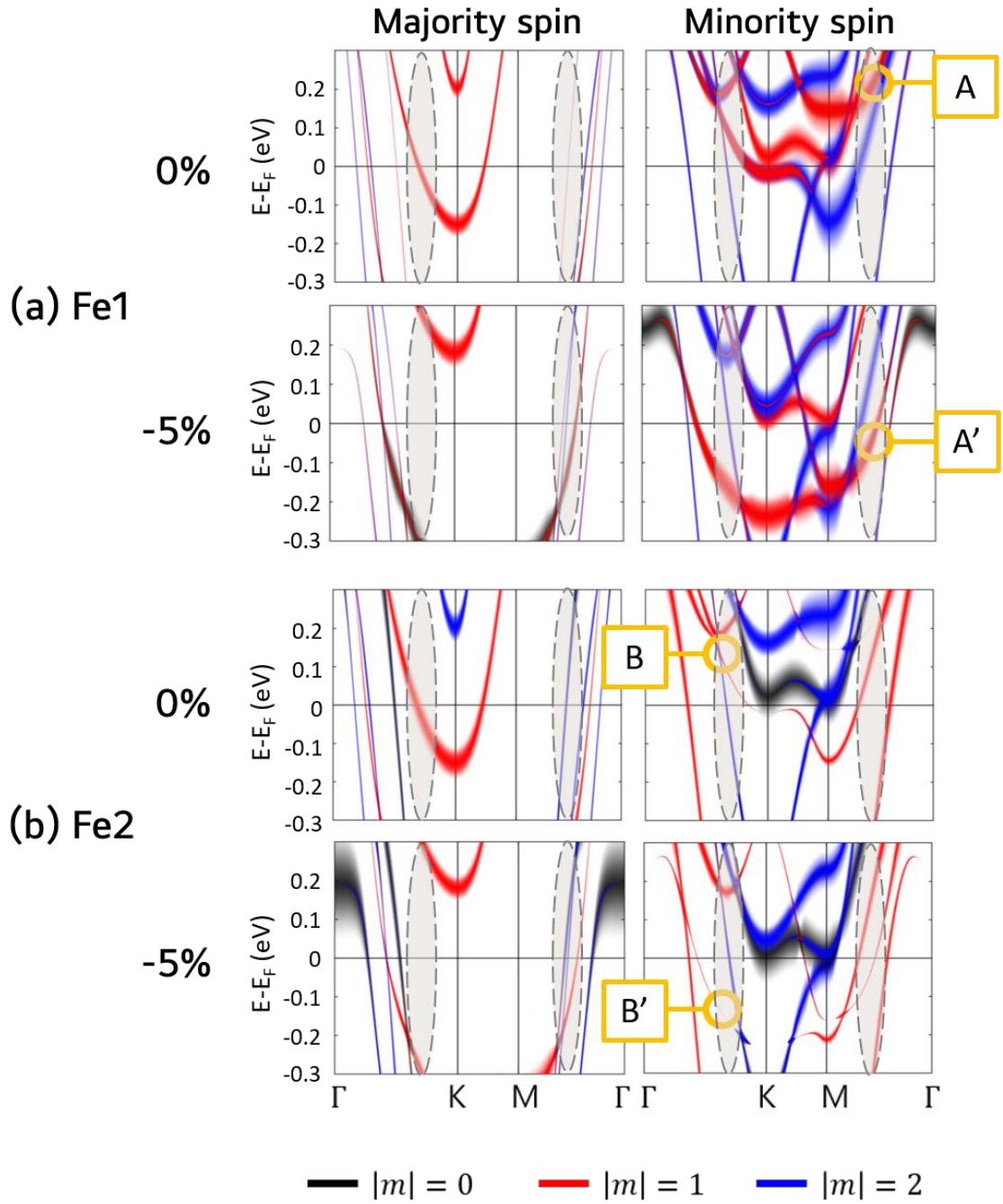


**Fig. 2.2.9** Band structures with orbital composition. Black stands for  $|m| = 0$ , red for  $|m| = 1$ , blue for  $|m| = 2$ , respectively. Contribution from (a) Fe1 and (b) Fe2 are distinguished. Highlight parts are same part as that of Fig. 2.2.8. Bands with occupation change under strain are denoted in yellow for Fe1 and Fe2, respectively.

## 2.3 Bilayer

In this section, bilayer  $\text{Fe}_3\text{GeTe}_2$  is discussed for strain dependent magnetic configurations and magnetic moments.

### 2.3.1 Magnetic configurations

In bulk, FGT is antiferromagnetic with Neel temperature of 214 K [2]. Fig. 2.3.1 shows two spin configurations of bilayer FGT, A-type AFM (A-AFM) and FM. As G-type bilayer FGT is unstable, we do not consider here. Within collinear magnetism, each monolayer is FM. A-AFM is consisted of oppositely arranged two FM layers. Energies of two magnetic configurations, FM and A-AFM, are compared for strain ( $-5\% \leq \eta \leq 5\%$ ) by  $\Delta E = E_{FM} - E_{AFM}$ , where  $E_{FM}(E_{AFM})$  stands for total energy of FM(AFM). Energy cutoff 450 eV and  $21 \times 21 \times 1$  Monkhorst-Pack  $k$  mesh are used. LDA is used for the exchange-correlation potential with vdW-DF-optB86b to properly describe van der Waals interaction. A vacuum spacing between two layers of 13.6 Å is taken to remove spurious interaction between adjacent layers.

Fig. 2.3.2 shows  $\Delta E$  as function of strain. Without strain, A-AFM is favored energetically over FM by  $\Delta E=15.96$  meV. While A-AFM is favorable, A-AFM to FM transition occurs at  $\eta = +4.16\%$ .

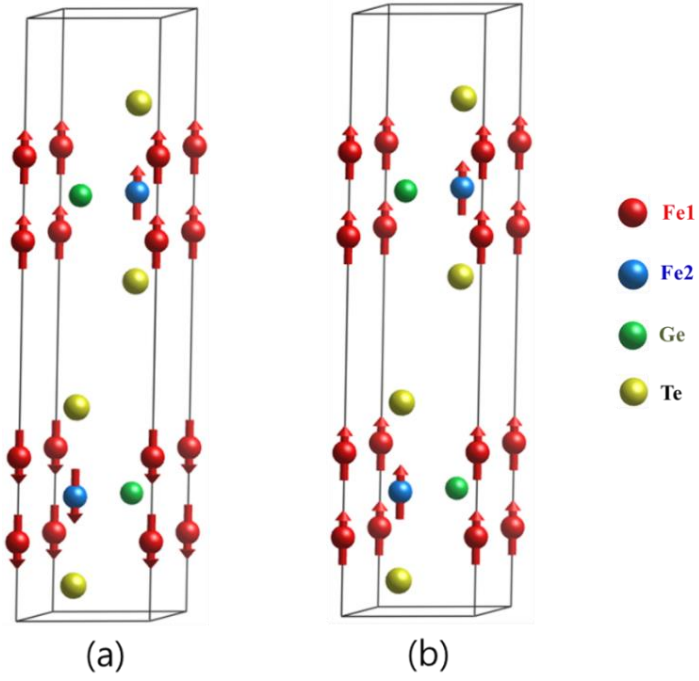


**Fig. 2.3.1** Two type of  $\text{Fe}_3\text{GeTe}_2$  spin configuration. (a) A-type antiferromagnetic state, (b) ferromagnetic state. Each monolayer has ferromagnetic state.

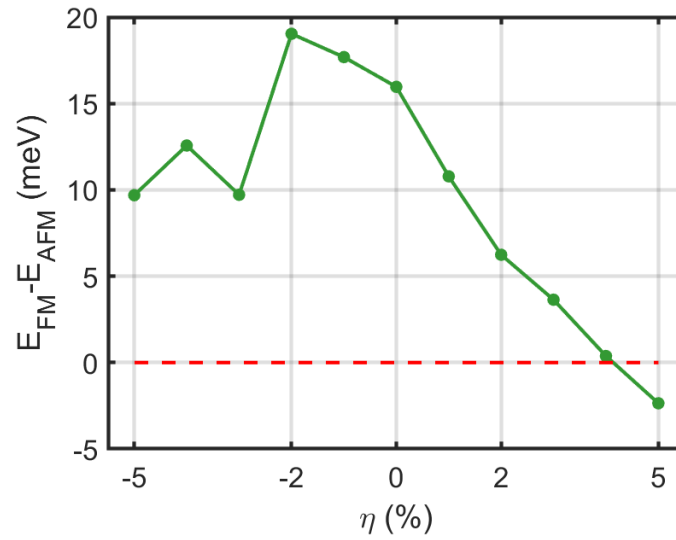


**Fig. 2.3.2** Energy difference between FM and A-AFM,  $\Delta E = E_{\text{FM}} - E_{\text{AFM}}$ , of bilayer  $\text{Fe}_3\text{GeTe}_2$ , with respect to strain.

### 2.3.2 Magnetic moments of Fe

Similar to monolayer case, strain also changes thickness of bilayer. In addition to thickness, Fe2-Ge buckling happens, which is illustrated in Fig. 2.3.3. The buckling occurs with compressive strain, where two Fe1 sites become inequivalent: Fe1(in)/Fe1(out) is closer to Ge/Fe2.

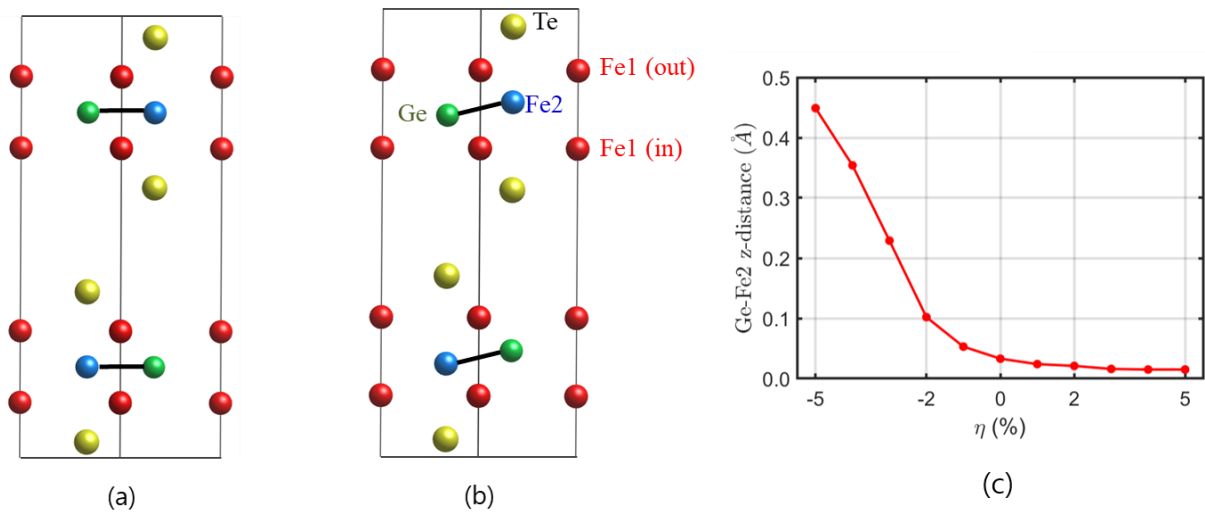


**Fig. 2.3.3** Structure of bilayer Fe<sub>3</sub>GeTe<sub>2</sub> (a) without strain and (b) with strain of -5%. In (b), with compressive strain, buckling happens in Fe2-Ge plane, where Fe2 and Ge move closer to Fe1(out) and Fe1(in), respectively. (c) Strain dependence of thickness of monolayer unit defined as distance between Fe2 z-axis position and Ge z-axis position.

In Fig. 2.3.4, magnetic moment of Fe2 changes little but that of Fe1 decreases (increases) with compressive (tensile) strain. More specifically, magnetic moment of Fe1(in) changes more than Fe1(out) with compressive strain. DOS of Fe1(in) and Fe1(out) at  $\eta = -5, 0$ , and  $5\%$  are plotted in Fig. 2.3.5 with their magnetic moments. Magnetic moment of Fe1(out) changes as much as  $\sim 0.2$  ( $-0.2$ )  $\mu_B$  from  $\eta = 0$  to  $5$  ( $-5$ )  $\%$ . On the other hand, Fe1(in) experiences drastic change at  $\eta = -5\%$ , as much as  $\sim 1.2$   $\mu_B$  from  $\eta = 0$   $\%$ . Fig. 2.3.5 shows DOS of three strains,  $\eta = -5, 0$ , and  $5\%$ , respectively. As seen,  $0$  and  $5\%$  strain exhibit quite similar: DOS of Fe1(in/out) are quite

similar. However, that in strain of  $-5\%$  is different. Different magnetic moments between Fe1(in) and Fe1(out) at  $-5\%$  is associated with different shape of DOS between them. More specifically, when  $\eta = 0$  and  $5\%$ , Fe1(in) has peak in empty state of the minority spin channel near  $E_F + 0.5$  eV. However, this kind of peak is absent when  $\eta = -5\%$ .

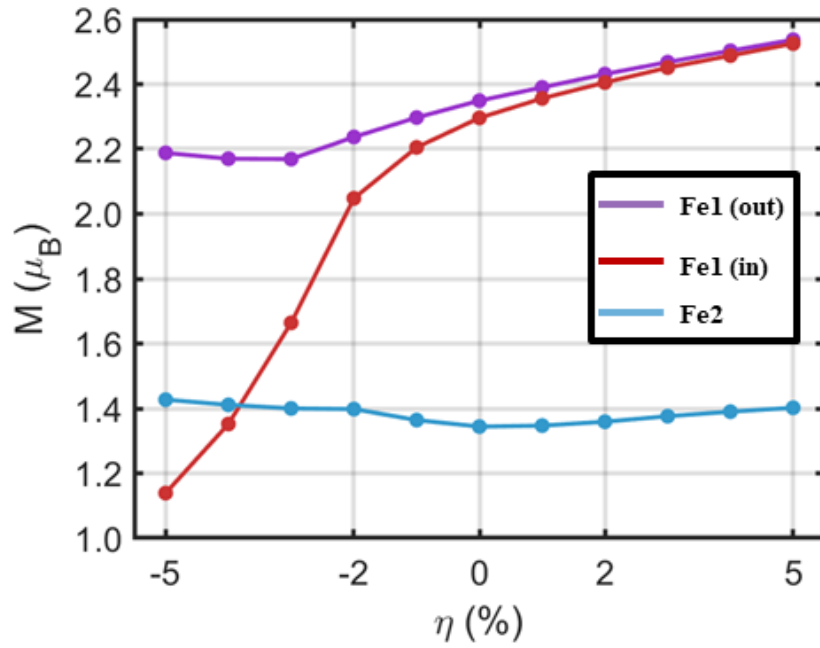


**Fig. 2.3.4** Bilayer  $\text{Fe}_3\text{GeTe}_2$  magnetic moment regarding strain. Purple, red and blue lines denote Fe1(out), Fe1(in), and Fe2, respectively. Fe2 magnetic moment is little changed. Fe1(in) magnetic moment is changed more than Fe1(out), especially in compressive strain range.

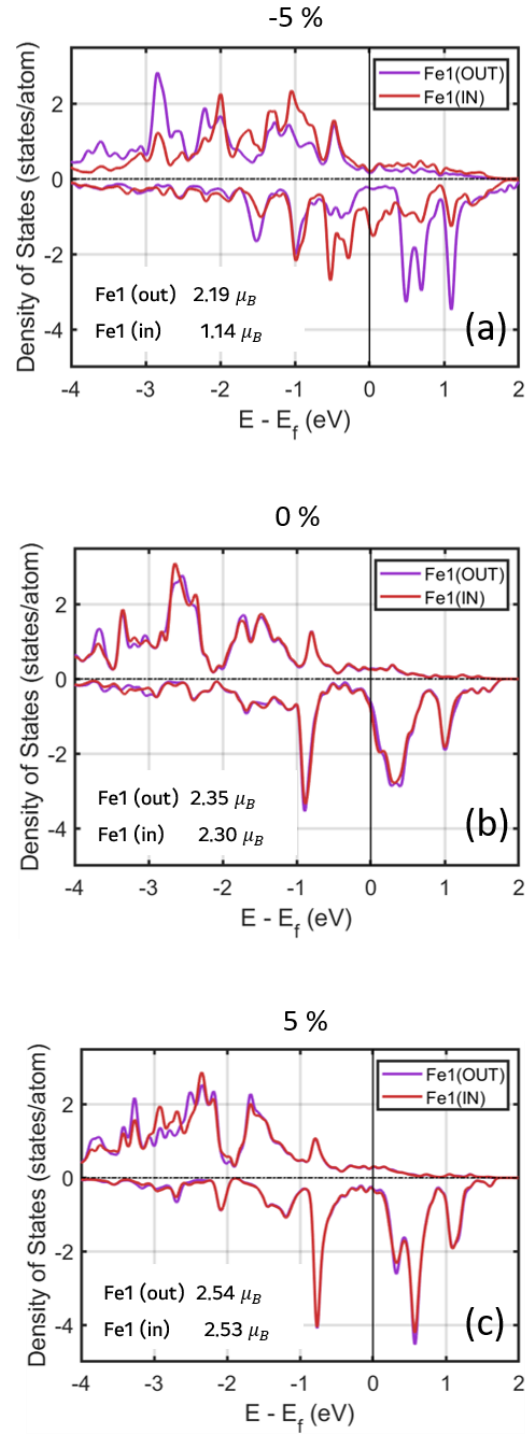


**Fig. 2.3.5** Density of states of Fe1(out) and Fe1(in) at strain of (a) -5, (b) 0, and (c) 5 %. The purple and red lines are Fe1(out) and Fe1(in), respectively. (b) and (c) show similar shape of DOS between Fe1(in) and Fe1(out) but (a) does not.

## 2.4 Reference

- [1] Zaiyao Fei, Bevin Huang, Paul Malinowski, Wenbo Wang, Tiancheng Song, Joshua Sanchez, Wang Yao, Di Xiao, Xiaoyang Zhu, Andrew F. May, Weida Wu, David H. Cobden, Jiun-Haw Chu and Xiaodong Xu, *Nat. Mater.* **17**, 778 (2018).
- [2] Jieyu Yi, Houlong Zhuang, Qiang Zou, Zhiming Wu, Guixin Cao, Siwei Tang, S A Calder, P R C Kent, David Mandrus and Zheng Gai, *2D Mater.* **4**, 011005 (2017).



## Chapter 3: Conclusion

In conclusion, using density functional theory, strain dependent magnetism has been presented for  $\text{Fe}_3\text{GeTe}_2$ , whose Curie temperature were reported 130 K and 180 K for monolayer and bilayer, respectively.  $\text{Fe}_3\text{GeTe}_2$  has hexagonal structure. Bilayer consists of two monolayer units connected by inversion symmetry.

For monolayer, we have discussed strain effect on magnetic moments and magnetocrystalline anisotropy. Among two Fe sites, Fe1 shows change of magnetic moments greater than Fe2. Density of states of strains,  $\eta = -5, 0$  and  $5 \%$ , exhibits different features. Furthermore, for all strains, monolayer  $\text{Fe}_3\text{GeTe}_2$  prefers perpendicular magnetization. In this regard, two strain of  $-5$  and  $0 \%$  with  $E_{MCA} = 0.85$  and  $4.72$  meV, respectively, are compared with band structure analysis.

For bilayer, we have discussed strain effect on magnetism. With two ferromagnetic monolayers, bilayer  $\text{Fe}_3\text{GeTe}_2$  prefers antiferromagnetism energetically at  $\eta = 0$ . At strain of  $+4.16 \%$ , transition from antiferromagnet to ferromagnet occurs. Moreover, buckling happens in Fe2-Ge plane at compressive strain. Fe2/Ge moves closer to Fe1(out) /Fe1(in), where two Fe1 sites show different magnetic moments regarding to strain. Density of states of Fe1(in) and Fe1(out) are compared at  $\eta = -5, 0$ , and  $5 \%$ .

## 국문 요약

밀도 범함수 이론을 이용하여 이차원 자성체  $\text{Fe}_3\text{GeTe}_2$ 의 변형에 의존하는 자성 특성에 대해 조사하였다.  $\text{Fe}_3\text{GeTe}_2$ 은 130 K 와 180 K의 퀴리 온도를 각각 단층과 이중층에서 가진다.  $\text{Fe}_3\text{GeTe}_2$ 는 육방 구조를 가지며 이중층 일 때 단층 간의 반전 대칭을 가지고 있다.

단층  $\text{Fe}_3\text{GeTe}_2$ 에 관해서, 자기모멘트와 결정자기이방성에 작용되는 변형의 효과에 대해 조사하였다. 변형에 따른 자기모멘트의 변화는  $\text{Fe1}$ 이  $\text{Fe2}$ 보다 더 크게 나타났다. 이와 관련하여  $\eta = -5, 0$  그리고 5 %에서의 상태밀도를 비교해보면 다른 특성을 나타내는 것을 알 수 있다. 또한 단층  $\text{Fe}_3\text{GeTe}_2$ 는  $-5 \leq \eta \leq 5$ 의 변형 범위 내에서 수직한 결정자기이방성을 선호한다. 이와 관련하여  $\eta = -5$ 와 0 %에서의 에너지 띠구조를 그들의 총 결정자기이방성 에너지 0.85, 4.72 meV와 함께 분석하였다.

이중층  $\text{Fe}_3\text{GeTe}_2$ 에 관해서, 변형에 따른 자성의 변화에 대해 조사하였다. 변형을 주지 않았을 때, 이중층은 강자성체 단층을 가지고 반강자성체 결합을 에너지적으로 선호한다. +4.16 %의 변형을 주게 되면, 반강자성체에서 강자성체로의 전이가 일어난다. 압축 변형을 주게 되면  $\text{Fe2-Ge}$  층에서 비틀림이 일어나서  $\text{Fe2/Ge}$ 은  $\text{Fe1(out)}/\text{Fe1(in)}$ 으로 가까이 움직인다. 나뉘어진 두  $\text{Fe1}$ 들은 변형에 따라 다른 자기모멘트의 변화를 보인다. 이와 관련하여  $\eta = -5, 0$  그리고 5 %에서의 상태밀도를 비교하여 분석하였다.